PROCEEDINGS, 42nd Workshop on Geothermal Reservoir Engineering
Stanford University, Stanford, California, February 13-15, 2017
SGP-TR-212

Comparison of a Fully Implicit and Sequential Implicit Formulation for Geothermal Reservoir Simulations

Zhi Yang WONG, Ruslan RIN, Hamdi TCHELEPI, Roland HORNE

Department of Energy Resources Engineering, Stanford University, Stanford, CA 94305

zhiyangw@stanford.edu

Keywords: Sequential formulation, fully implicit, geothermal reservoir simulation, convergence

ABSTRACT

This study compared the fully implicit formulation and sequential formulation for geothermal reservoir simulation. In particular, we looked at how the choice of coupling terms affects the nonlinear convergence behavior. The main difference between the two formulations is that in the fully implicit formulation, the flow and thermal equations are solved together at the nonlinear level, while for the sequential formulation, the flow and thermal equations are solved separately and coupled iteratively with a coupling term. These formulations were implemented in the Automatic-Differentiation General Purpose Research Simulator (AD-GPRS). AD-GPRS has a general implicit coupling framework for multi-physics problems and provides a unified interface for both formulations. This ensures that the differences in performances are isolated to be a result of the formulation rather than implementation issues. The performance of the formulations was quantified in terms of the time-step size and the number of Newton and sequential iterations for each coupled approach. The results from the numerical experiments showed that fully implicit method performs significantly better than all sequential schemes. We found that a hybrid method having a constant pressure for single-phase blocks and constant density for two-phase blocks performed the best out of all the sequential schemes.

1. INTRODUCTION

Computational modeling of geothermal reservoirs is an essential part of the development and management of any geothermal field (O'Sullivan et al., 2001). The complexities stemming from the geology and physics of geothermal reservoir models results in significant issues of numerical convergence for these simulations (Magnusdottir 2013, Noy et al. 2012). This issue of numerical convergence is exacerbated in inverse modeling and uncertainty quantification where an ensemble of simulations are performed, thus, the need for robust and fast converging solutions are required for problems with practical interest.

One of the main challenges for convergence in geothermal simulations is the tight coupling between the flow and thermal equations. This coupling is mainly through the thermodynamic relationships that govern the fluid that each block has to satisfy. Due to this tightly coupled nature of the flow and thermal equations, the industry standard (Pruess et al., 1999, Zaydullin et al., 2014) is to use a fully implicit approach to ensure stability in the solution. Although this guarantees numerical stability in the solution, this does not guarantee nonlinear convergence. To add to the complexity of the tightly coupled flow and thermal equations, these equations exhibit both parabolic and hyperbolic behavior – parabolic in flow and conduction, hyperbolic in the transport terms. This complexity makes analyzing the entire nonlinear problem difficult. A separation of the different physics could improve the understanding and result in a better design of nonlinear solvers for the geothermal problem.

To separate the parabolic and hyperbolic parts of the flow and thermal equations, there has been work done previously (Trangenstein, 1989, van Odyck et al., 2009) that implemented a sequential formulation rather than the typical fully implicit approach. Trangenstein (1989) and van Odyck et al. (2009) analyzed the sequential method for thermal problems. The focus of their formulations was to demonstrate the ability for pressure to be solved implicitly followed by an explicit solve for enthalpy. Due to the explicitness of enthalpy, all the numerical tests were conducted for a CFL < 1 (See Equation 8 for the definition of CFL). This CFL is relatively low in comparison to the CFL size that obtainable for complex fully implicit isothermal problems (Wang and Tchelepi 2013, Li and Tchelepi 2015, Hamon et al., 2015).

This sequential formulation approach has also been applied to the coupling between flow and geomechanics. The literature regarding the sequential coupling between the geomechanics and flow parts of the problem is significantly more extensive (Settari et al. 1998, Kim et al., 2009, Mikelic and Wheeler, 2013, Castelletto et al., 2015). The sequential formulation is more common for the flow and geomechanics as the flow and geomechanics have different domain size (geomechanics domain is usually much larger than the flow part) and different space discretization methods (finite volume for flow and finite element for geomechanics). Additionally, finding an efficient preconditioner for the fully coupled flow-geomechanics problem is an active area of research (Castelletto et al., 2015), while there are efficient preconditioners for separated flow and geomechanics (Cao et al., 2005). These difficulties make the use of specialized simulators for each physics an attractive alternative option (e.g. coupling TOUGH2 for flow (Pruess et al., 1999) and FLA3D for geomechanics (Rutqvist et al., 2002)).

There are several ways of coupling flow and geomechanics problems: fixed-stress split, fixed-strain split, drained and undrained split (Kim et al., 2011a, Kim et al., 2011b). It has been shown mathematically that the fixed-stress scheme is unconditionally stable and

convergent (Kim et al., 2009) and performs the best among all of them. The fixed-stress scheme is the case where the flow is solved first followed by the mechanical problem coupled with stress component; these two problems are solved iteratively until convergence is obtained. However, due to the tightly coupled nature of the flow and thermal equations, most schemes use a fully implicit approach and to the best of our knowledge, a similar analysis for flow and thermal problems is limited. In addition, both flow and thermal problems are often solved with a finite volume scheme; this makes fully coupled formulation an appealing choice for implementation.

The strong coupling between the flow and thermal equations makes the full nonlinear problem difficult to analyze. The common approach to performing such analysis is to decouple the different nonlinearities such that each individual nonlinearity is analyzed separately. For isothermal problems, the pressure and saturation equations are solved separately to investigate the flux function for the hyperbolic saturation equation. This flux function has been a key to understanding the nonlinearities for these nonlinear isothermal simulation problems. Jenny et al. (2009) developed a nonlinear solver based upon the saturation equation for isothermal two-phase flow. They used the analytical flux function to determine where the inflection point and thus guide their Newton solver for saturation updates. Wang and Tchelepi (2013) extended this approach to two-phase problems with viscous and buoyancy forces by using a 'trust-region' type solver to determine which saturation values the Newton's method was guaranteed to converge. These intervals were based upon the inflection points and unit flux points of the analytical flux function. Li and Tchelepi (2015) improved upon the analysis of Wang and Tchelepi (2013) to show that these trust regions should be computed for the numerical and not for the analytical flux.

The purpose of this work was to conduct a preliminary study on the sequential fully implicit scheme for the flow and thermal conservation equations to give insight as to how the different nonlinearities and physics could be decoupled. We compared three sequential coupling schemes against the fully implicit scheme. We examined the performance of each coupling scheme on three test cases. This is similar to the work done by Kim et al. (2009) where different coupling strategies were investigated for the flow-geomechanics problem; however, this work looked solely on numerical examples. The implementation and simulation framework used for this study follows on from previous work in Wong et al. (2015) and Wong et al. (2016).

2. NUMERICAL FORMULATION

2.1 Governing Equations

For this study, we consider only the flow and transport of pure water in two-phase flow. The flow and thermal are the mass and energy conservation equations denoted by F and T correspondingly:

$$F = \frac{\partial}{\partial t}\left(\phi(\rho_w S_w + \rho_s S_s)\right) - \nabla.(\rho_w u_w + \rho_s u_s) - Q_F = 0 \tag{1}$$

$$T = \frac{\partial}{\partial t}\left((1-\phi)\rho_R U_R + \phi(\rho_w U_w S_w + \rho_s U_s S_s)\right) - \nabla.(\rho_w h_s u_w + \rho_s h_s u_s) - \nabla.(K\nabla T) - Q_T = 0 \tag{2}$$

where:

- ϕ is the porosity of the rock
- ρ_k is the mass density of phase k
- S_k is the saturation of phase k
- u_k is the velocity of phase k
- Q is the source/sink term
- h_k is the enthalpy of phase k
- U_k is the internal energy of phase k
- K is the total conductivity of the fluid and rock

Here the subscripts w/s represents the two phases water and steam, and the subscript R represents the rock. Both ρ_k, h_k in each phase depend on the phase state of the fluid. The thermodynamic parameters that were used for this study had all the parameters as a function of p and h of the block (Faust and Mercer, 1979).

In addition to these two conservation equations, the saturation constraint must be satisfied, the sum of all the phase saturations is equal to one.

$$S_w + S_s = 1 \tag{3}$$

2.2 Darcy's Law

To model the velocity of each phase, Darcy's law was used to describe the flow through the porous media:

$$u_k = \frac{k k_{rk}}{\mu_k}\nabla(p_k + \rho_k g z) \tag{4}$$

where:

- u_k is the superficial velocity of phase k

- k is the rock permeability
- k_{rk} is the relative permeability of phase k
- μ_k is the viscosity of phase k
- p_k is the pressure of phase k
- g is the gravitational constant
- z is the direction of the gravity
- k represents either the water phase or steam phase

The two-point flux approximation (TPFA) finite volume method and a fully implicit method was implemented to discretize the flow and thermal conservation equations (Equations 1 and 2) in space and time. The analysis for this entire study used the phase-based, single-point upstream-weighted TPFA scheme.

2.2 Fully Coupled Formulation

The finite volume approximation results in the system of nonlinear equations for flow and thermal problems:

$$R_F^{n+1}(x_F^{n+1}, x_T^{n+1}) = \left(\phi(\rho_w S_w + \rho_s S_s)\right)^{n+1} - \left(\phi(\rho_w S_w + \rho_s S_s)\right)^{n} - \nabla.(\rho_w u_w + \rho_s u_s)^{n+1} - Q_F^{n+1} = 0 \tag{5}$$

$$\begin{aligned} R_T^{n+1}(x_F^{n+1}, x_T^{n+1}) = {} & \left((1-\phi)\rho_R U_R + \phi(\rho_w U_w S_w + \rho_s U_s S_s)\right)^{n+1} - \left((1-\phi)\rho_R U_R + \phi(\rho_w U_w S_w + \rho_s U_s S_s)\right)^{n} \\ & - \nabla.(\rho_w h_s u_w + \rho_s h_s u_s)^{n+1} - \nabla.(K\nabla T)^{n+1} - Q_T^{n+1} = 0 \end{aligned} \tag{6}$$

Here the superscript x_F^{n+1}, x_T^{n+1} represents the primary variables for the flow and thermal equations at the time level $(n+1)$. The typical fully implicit method solves all the residual equations simultaneously:

$$\begin{aligned} R_F^{n+1}(x_F^{n+1}, x_T^{n+1}) &= 0 \\ R_T^{n+1}(x_F^{n+1}, x_T^{n+1}) &= 0 \end{aligned} \tag{7}$$

Using Newton's method to solve this system of nonlinear equations this leads to:

$$\begin{bmatrix} \dfrac{\partial R_F}{\partial x_F} & \dfrac{\partial R_F}{\partial x_T} \\ \dfrac{\partial R_T}{\partial x_F} & \dfrac{\partial R_T}{\partial x_T} \end{bmatrix} \begin{bmatrix} \delta x_F \\ \delta x_T \end{bmatrix} = - \begin{bmatrix} R_F \\ R_T \end{bmatrix} \tag{8}$$

2.3 Fully Implicit Sequential Formulation

For the fully implicit sequential formulation, the flow and thermal equations are solved separately for the respective primary variables x_M, x_T and a coupling variable is used to allow each equation to be solved. For this study, we only examined using a pressure-enthalpy formulation as described in Wong et al. (2016). The pressure-enthalpy formulation does not require any variable switching and thus allows for a simpler implementation and analysis of this fully implicit sequential formulation. It is important to note that this sequential formulation is iteratively coupled until convergence for both the flow and energy equation, thus the converged solution will be identical for both formulations within the desired tolerance.

We will first describe the sequential fully implicit method for flow and thermal with general coupling terms and then specify different coupling terms. Figure 1 shows an overview of the entire algorithm.

Step 1: Solve:

$$R_F^{n+1}(x_F^{n+1}, x_T(\delta c_F^{n+1} = 0)) = 0 \tag{9}$$

This involves solving the flow equation with a variable $\delta c_F = 0$. This variable is the constant variable that we assume is fixed while we solve the flow equation. The choice of variable for c_F affects the convergence and stability of the coupled system. Here, we assume $c_F \equiv h$ (the fluid enthalpy of the system) for all cases, while $x_F = p$. Once we have the solution x_F^{n+1,k^*} (k^* – is index of sequential iteration), we use that as the initial guess to the solution of the thermal equation.

Step 2: Solve:

$$R_T^{n+1}(x_F(\delta c_T^{n+1} = 0), x_T^{n+1}) = 0 \tag{10}$$

This involves solving the thermal equation with a variable $\delta c_T = 0$. Similar to c_F, variable c_T is constant when solving the thermal equation. The choice of c_T is the primary focus of this work. Once the thermal equation is solved with Newton's method, Step 1 (Equation 9) and 2 (Equation 10) are repeated until convergence.

Algorithm 1 Sequential Method

$p^{\nu} = p^n, h^{\eta^*} = h^n$
while $||[R^F; R^T]||_2 > \epsilon_R$ **do**
  while $||R^F||_2 > \epsilon_F$ **do** (Step 1)
    $dp = -J_F(p^{\nu}, h^{\eta^*})^{-1} R_F$
    $p^{\nu+1} = p^{\nu} + dp$
  end while
  $p^{\nu^*} = p^{\nu+1}$
  $c_T^{\nu^*} = c_T(p^{\nu^*}, h^{\eta^*})$
  while $||R^T||_2 > \epsilon_T$ **do** (Step 2)
    $dh = -J_T^{-1}(c_T^{\nu^*}, h^{\eta}) R_T(p^{\nu^*}, h^{\eta})$
    $h^{\eta+1} = h^{\eta} + dh$
  end while
  $h^{\eta^*} = h^{\eta}$
  $p^{\nu} = p(c_T^{\nu^*}, h^{\eta^*})$
end while

Figure 1: Algorithm for the sequential method $\left(\boldsymbol{x_F = p, x_T = h, J_F = \frac{\partial R_F}{\partial p}, J_T = \frac{\partial R_T}{\partial h}}\right)$

2.4.1 Constant Pressure

The constant pressure scheme assumes the pressure is constant ($c_T \equiv p$) in the thermal residual equation. Thus Equation 10 is:

$$R_T^{n+1}\left(x_F = x_F^{n+1,k^*}, x_T^{n+1}\right) = 0 \tag{11}$$

where x_F^{n+1,k^*} is the solution of the flow residual equation sequential solve. This is the same as solving the solution with $\frac{dp}{dh} = 0$.

2.4.2 Constant Density

For the constant density formulation, rather than assuming a constant pressure, each block is assumed to have a constant total density($c_T \equiv \rho$). We first compute the density of the solution of the flow sequential solve and use that value to update our solution in the thermal residual equation:

$$R_F^{n+1}\left(x_T(\rho^{n+1,^*}), x_T^{n+1}\right) = 0 \tag{12}$$

In order to do this in the general sense, we use the Inverse Function to get the derivatives of pressure with enthalpy:

$$\frac{dp}{dh}(\delta\rho = 0) = \frac{dF}{dh}\left(\frac{dF}{dp}\right)^{-1} \tag{13}$$

where:

$$F(p, h) = \rho^{n+1,k^*} - \rho(p, h) = 0 \tag{14}$$

Here, we have p, h are the pressure and enthalpy of the fluid and ρ is the thermodynamic relationship that computes the density as a function of pressure and enthalpy. ρ^{n+1,k^*} is the density of the converged solution of the flow equation (Equation 9).

2.4.3 Constant Pressure and Constant Density (Hybrid)

The final formulation is a combination of the constant pressure and constant density formulation. We will refer to this formulation as the hybrid formulation. This mixed formulation is dependent on the phase state of the block. For this formulation, we chose a constant pressure coupling term for the single-phase blocks and constant density for the two-phase blocks. We define the phase-state of the block by comparing the h with the saturated enthalpy of the block $h_w(p)$ and $h_s(p)$. More formally, we define the coupling term as:

$$c_T \equiv \begin{cases} \rho, & h_w(p) \le h \le h_s(p) \\ p, & \text{otherwise} \end{cases} \tag{15}$$

3. IMPLEMENTATION

3.1 AD-GPRS

The implementation and investigations for this study were completed using Automatic-Differentiation General Purpose Research Simulator (AD-GPRS) (Voskov and Tchelepi, 2012, Zhou, 2012). AD-GPRS provides a general implicit coupling framework for solving multi-physics problems (Rin et al., 2017). The framework employs modular design for each physics, and allows the development and testing different coupling strategies within a unified interface. Such approach greatly reduces efforts to implement each strategy and ensures consistent performance comparison between different coupling schemes. This work integrates the geothermal module into the new AD-GPRS framework (Wong et al., 2016).

In addition to the general implicit coupling framework, AD-GPRS has a wide range of capabilities in advanced physical modeling and numerical methods. These capabilities include thermal-compositional, EOS-based, multiphase flow and transport models (Zaydullin et al., 2014; Voskov et al., 2016), generalized nonlinear formulations (Voskov, 2012, Zaydullin et al., 2013), multistage linear solvers (Zhou et al., 2013, Klevtsov et al., 2016), complex multi-segment wells (Zhou, 2012), and nonlinear mechanical deformation models (Garipov et al., 2015, 2016).

NUMERICAL COMPARISONS

Here we consider different problems with varying complexity. The verification of the fully implicit results was shown in Wong et al., (2015) and Wong et al., (2016) where the fully implicit results were compared with analytical, semi-analytical and TOUGH2 simulations. Here the focus is to compare the convergence properties of the different sequential formulations with the fully implicit solution.

We use a direct linear solver PARDISO (Petra et al., 2014a, 2014b, Schenk and Gärtner, 2004) to isolate the effects of the linear solver solution on the nonlinear solver. In all the cases, the maximum sequential iterations was set to be 30, the maximum nonlinear iterations was set to 20, the convergence tolerance for the flow and thermal equations was set to 10^{-4}.

4.1 One-dimensional Radial Model

This numerical model is a one-dimensional, radial model. The single-phase cases involve the injection or production in the radial model where the fluid remains completely as single-phase liquid water. The two-phase case involves the propagation of a flash front moving outwards, either a cold-water front for injection or the propagation of a two-phase zone for production.

The rock parameters for this model are defined as:

Table 1: Rock and geometry parameters for the model

Porosity	0.2
Permeability (md)	10
Thickness (m)	100
Rock Compressibility	0
Rock thermal conductivity	0

The Corey curves were used as the relative permeability relationships:

$$k_{rl} = (S^*)^4$$
$$k_{rg} = ((1 - S^*)^2(1 - (S^*)^2) \quad (16)$$
$$S^* = \frac{S_w - 0.3}{0.65}$$

where k_{rl} is the relative permeability of liquid is water and k_{rg} is the relative permeability of the steam.

The same discretization scheme was used as in the code comparison study where the radius of each segment was:

$$r_n = 0.5 \times 2^{\frac{n-1}{2}} m, n = 1,2,3,\dots,25 \quad (17)$$

The pressure and temperature for all the different cases can be found in Appendix A. There is a significant difference in the pressure solutions for the cases that had numerical issues due to different time stepping schemes for each formulation.

Table 2: Initial reservoir condition and well constraints for each of the scenarios

	Production 1	**Injection 1**	**Production 2**	**Injection 2**
Phases present	Liquid Water	Liquid Water	Two-phase	Two-phase
Initial pressure (bars)	90	45	90	10
Initial temperature (°C)	250	250	300	282

Initial water saturation	1.0	1.0	1.0	0.1
Production rate (m^3/s)	-	-	14.0	-
BHP well (bar)	45	90	-	90
Injection Temperature (°C)	-	250	-	82

The maximum time step was compared to the two formulations for a production scenario. We will compare the time step size in terms of a CFL number, for the single block case it is defined as:

$$CFL_{max} = \frac{\Delta t Q}{PV} \tag{18}$$

where:

- Δt is the maximum time step
- Q is the volume injection rate
- PV is the pore volume of the block

4.1.1 Single-phase

In the single-phase production case, the constant pressure and hybrid scheme achieved identical nonlinear performance. This is because the entire domain remains in single-phase water throughout the entire simulated period thus the coupling property is pressure for all the blocks. For both the constant pressure, hybrid and fully implicit method, there were no time step cuts and the predefined maximum CFL of 100 was reached for all schemes. For the constant density case, the maximum CFL was about an order of magnitude less than the other three schemes.

Identically to the production case, for the single-phase injection case, the constant pressure and hybrid scheme obtained identical nonlinear performance. For both the constant pressure, hybrid and fully implicit method again there were no time step cuts. For the constant density case, the maximum CFL was about two orders of magnitude less than the other three schemes.

Table 3: Comparison between sequential coupling schemes for single-phase one-dimensional production scenario

	Constant Pressure	**Constant Density**	**Hybrid**	**Fully Coupled**
Number Time Steps	27	62	27	27
Total Newton Iterations	37	2176	37	15
Total Sequential Iterations	50	2285	50	-
Wasted Time Steps	0	40	0	0
Wasted Newton Iterations	0	2637	0	0
MaxCFL	100	12.3	100	100

Table 4: Comparison between sequential coupling schemes for single-phase one-dimensional injection scenario

	Constant Pressure	**Constant Density**	**Hybrid**	**Fully Coupled**
Number Time Steps	63	2128	63	63
Total Newton Iterations	694	54228	694	122
Total Sequential Iterations	291	93876	291	-
Wasted Time Steps	0	2119	0	0
Wasted Newton Iterations	0	127015	0	0

MaxCFL	87.7	1.2	87.7	87.7

4.1.3 Two-phase

For the two-phase case, the constant pressure case was diverging and the sequential iterations did not converge for a reasonable time step that allowed the simulation to run to completion. The constant density and constant hybrid had nearly identical solutions for the production scheme because most of the nonlinearity occurred at the front of production flash front. For the fully implicit case, the production scenario again did not have any difficulty and there were zero wasted time steps.

For the injection case, the hybrid case performed the best with the largest CFL number and with the lowest number of time step cuts. It is interesting to note that the hybrid method performed better than the fully implicit case for the injection case. Although the constant density case converges, it is again one order of magnitude worse than the hybrid and fully implicit case.

Table 5: Comparison between sequential coupling schemes for two-phase one-dimensional production scenario

	Constant Pressure	**Constant Density**	**Hybrid**	**Fully Coupled**
Number Time Steps	Sequential solution diverges	62	61	26
Total Newton Iterations		2176	2078	71
Total Sequential Iterations		2285	2203	-
Wasted Time Steps		40	39	0
Wasted Newton Iterations		2637	2580	0
MaxCFL		9.2	9.2	30.4

Table 6: Comparison between sequential coupling schemes for two-phase one-dimensional injection scenario

	Constant Pressure	**Constant Density**	**Hybrid**	**Fully Coupled**
Number Time Steps	Sequential solution diverges	881	61	79
Total Newton Iterations		23432	906	316
Total Sequential Iterations		38566	373	-
Wasted Time Steps		870	7	31
Wasted Newton Iterations		53104	7	88
MaxCFL		7.4	98.3	93.1

4.3 Two-dimensional Heterogeneous Single-Phase

The distribution of permeability and porosity were taken from the top layer of the SPE10 model, the permeability distribution can be seen in Figure 2 (Christie and Blunt, 2001). There are $60 \times 60 \times 1$ grid blocks, each grid block is $20 \times 10 \times 70$m. The scenario was constantly at single-phase. Only the single-phase case was tested because the fully implicit case was already found to struggle with the heterogeneous multiphase solution. The purpose of these test cases was to compare how the best sequential formulation would compare with the fully implicit case for more complicated scenarios. This is a highly heterogeneous permeability field and stresses how the sequential formulation handles strong contrasts in permeability.

4.3.1 Production

For the production scenario, uniform pressure (100 bars), temperature (523.15 K) and water saturation (1.0) were imposed as the initial conditions. A single production bottom hole pressure (45 bars) controlled well was located in the center of the reservoir. The production case was run for 100 days and the injection was run for 500 days.

4.3.2 Injection

For the injection scenario, uniform pressure (45 bars), temperature (523.15 K) and water saturation (1.0) were imposed as the initial conditions. A single injection bottom hole pressure (100 bars) controlled well was located in the center of the reservoir. The production case was run for 100 days and the injection was run for 500 days.

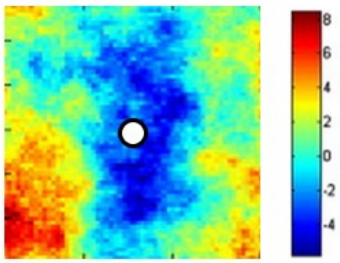

Figure 2: Log of permeability (md) distribution of a section of the top layer of the SPE 10 model (White dot represents the production or injection well)

4.3.3 Results

The hybrid method had worse results in the production and injection scenarios. For the production scenario, the results were comparable (MaxCFL of 30.1 compared with 46.3) to the fully implicit case. However, for the injection scenario, the fully implicit case was two orders of magnitude better than the fully implicit case. It is clear from these two cases that the sequential formulation is performing worse than the fully implicit case for this two-dimensional heterogeneous case.

Table 7: Comparison between the sequential and fully implicit method for single-phase two-dimensional heterogeneous production scenario

	Hybrid	**Fully Coupled**
Number Time Steps	42	30
Total Newton Iterations	76	29
Total Sequential Iterations	487	-
Wasted Time Steps	13	0
Wasted Newton Iterations	624	0
MaxCFL	30.12	46.31

Table 8: Comparison between the sequential and fully implicit method for single-phase two-dimensional heterogeneous injection scenario

	Hybrid	**Fully Coupled**
Number Time Steps	774	51
Total Newton Iterations	15421	68
Total Sequential Iterations	31814	-
Wasted Time Steps	741	0
Wasted Newton Iterations	30938	0
MaxCFL	1.43	100.4

4.4 Three-dimensional model with phase change

The last case is a three-dimensional model based on a reservoir model from the 1980 Code Comparison Study (Stanford Geothermal Program, 1980). The reservoir model consists of single-phase liquid water with a two-phase zone of immobile steam sandwiched between a hot and cold water region. Production is performed from a well that is completed below the two-phase zone. The parameters were chosen such that the boiling in the well occurs after a certain period of production. Although the parameters are relatively homogeneous, it was used as a prototype for field-wide reservoir development studies. This problem has both three-dimensional flow with phase transitions and two-phase flow, including gravity drainage. A full discussion on the problem description can be found in Stanford Geothermal Program (1980). This was coarsened test case in comparison to the one used in Wong et al. (2016).

The only change in this problem is that this computational grid had $20 \times 25 \times 30$ total blocks that were $200 \times 200 \times 60\ m$ in size. The production well was completed in the corner block and perforates layers 16-20. The water rate at $100 m^3$/day was used as the well control. The simulation time was for 500 days.

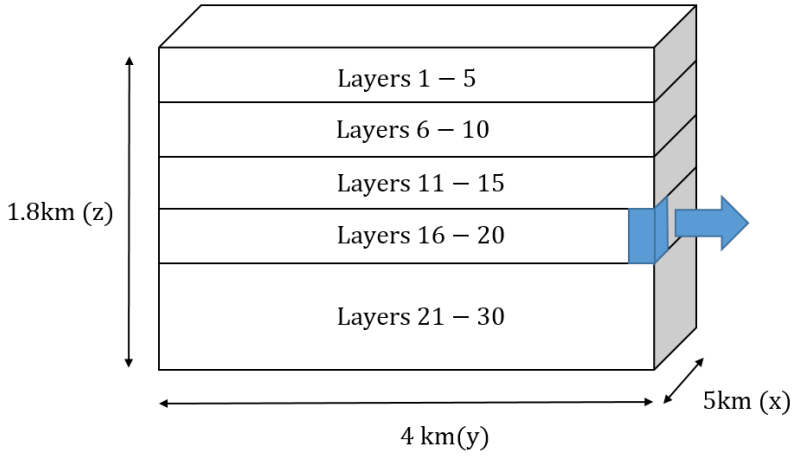

Figure 3: Schematic of the three-dimensional model

Similar to the two-dimensional heterogeneous case, the hybrid formulation performs worse than the fully implicit case. Again the performance is about two orders of magnitude worse than the fully implicit case. This can be observed by the CFL being about two orders of magnitude worse than the fully implicit case. It is important to note that the fully implicit case did not have any wasted time steps and a more aggressive time stepping scheme could actually provide better results for the fully implicit method.

Table 9: Comparison between the sequential and fully implicit method for three-dimensional model

	Hybrid	**Fully Coupled**
Number Time Steps	1392	21
Total Newton Iterations	1217	35
Total Sequential Iterations	4569	0
Wasted Time Steps	1382	0
Wasted Newton Iterations	29944	0
Max CFL	0.4	11.9

5. DISCUSSION AND CONCLUSIONS

Using a general implicit coupling framework, we investigated the convergence properties for three different sequential coupling schemes. It was found that a hybrid method where the coupling property was pressure for single-phase blocks and density for two-phase blocks performed the best out of the three that were tested. This hybrid method was able to avoid the divergent or slow converging behavior in the single-phase (constant density) or two-phase (constant pressure) regions. More numerical tests also showed that the fully implicit method performed significantly better than the sequential scheme. This difference was more pronounced for the two-dimensional and three-dimensional models. These comparisons and analysis on the sequential scheme were only performed for numerical tests. Mathematical analysis of the different coupling schemes is ongoing research. The further mathematical analysis could provide insight as to how to design better nonlinear solvers for the fully implicit solution.

ACKNOWLEDGEMENTS

Funding by the Industrial Affiliates Consortium on Reservoir Simulation at Stanford University (SUPRI-B) is appreciated. The authors are grateful to Pavel Tomin valuable discussions and very helpful ideas.

REFERENCES

Cao, H., Tchelepi, H. A., Wallis, J. R., & Yardumian, H. E. (2005). Parallel scalable unstructured CPR-type linear solver for reservoir simulation. In SPE Annual Technical Conference and Exhibition. Society of Petroleum Engineers.

Castelletto, N., White, J. A., & Tchelepi, H. A. (2015). Accuracy and convergence properties of the fixed-stress iterative solution of two- way coupled poromechanics. International Journal for Numerical and Analytical Methods in Geomechanics, 39(14), 1593-1618.

Christie, M. A., & Blunt, M. J. (2001). Tenth SPE comparative solution project: A comparison of upscaling techniques. In SPE Reservoir Simulation Symposium. Society of Petroleum Engineers.

Faust, C. R., and Mercer, J. W. (1979). Geothermal reservoir simulation: 2. numerical solution techniques for liquid and vapor-dominated hydrothermal systems. Water Resources Research, 15(1):31–46.

Garipov, T., Voskov, D., and Tchelepi, H. A. (2015). Rigorous coupling of geomechanics and thermal compositional flow for SAGD and ES-SAGD operations. In SPE Canada Heavy Oil Technical Conference. Society of Petroleum Engineers.

Garipov, T. T., White, J., Lapene, A., and Tchelepi, H. A. (2016). Thermo-hydro-mechanical model for source rock thermal maturation. In 50th US Rock Mechanics / Geomechanics Symposium, Houston, USA. Society of Petroleum Engineers.

Hamon, F. P., Mallison, B., & Tchelepi, H. (2015). Hybrid Upwind Discretization for the Implicit Simulation of Three-Phase Coupled Flow and Transport with Gravity. In AGU Fall Meeting Abstracts.

Karypis, G., & Kumar, V. (1998). A fast and high quality multilevel scheme for partitioning irregular graphs. SIAM Journal on Scientific Computing, 20(1), 359-392.

Kim, J., Tchelepi, H. A., & Juanes, R. (2009). Stability, accuracy, and efficiency of sequential methods for coupled flow and geomechanics. In SPE reservoir simulation symposium. Society of Petroleum Engineers.

Kim, J., Tchelepi, H. A., & Juanes, R. (2011a). Stability and convergence of sequential methods for coupled flow and geomechanics: Fixed-stress and fixed-strain splits. Computer Methods in Applied Mechanics and Engineering, 200(13), 1591-1606.

Kim, J., Tchelepi, H. A., & Juanes, R. (2011b). Stability and convergence of sequential methods for coupled flow and geomechanics: Drained and undrained splits. Computer Methods in Applied Mechanics and Engineering, 200(23), 2094-2116.

Klevtsov, S., Castelletto, N., White, J. A., and Tchelepi, H. A. (2016). Block-preconditioned Krylov methods for coupled multiphase reservoir flow and geomechanics. In ECMOR XIV-15th European Conference on the Mathematics of Oil Recovery.

Li, B., & Tchelepi, H. A. (2015). Nonlinear analysis of multiphase transport in porous media in the presence of viscous, buoyancy, and capillary forces. Journal of Computational Physics, 297, 104-131.

Magnusdottir, L. (2013). Fracture Characterization in Geothermal Reservoirs Using Time-lapse Electric Potential Data. Ph.D. thesis, Stanford University.

Mikelić, A., & Wheeler, M. F. (2013). Convergence of iterative coupling for coupled flow and geomechanics. Computational Geosciences, 17(3), 455-461.

Noy, D., Holloway, S., Chadwick, R., Williams, J., Hannis, S., and Lahann, R. (2012). Modeling large-scale carbon dioxide injection into the Bunter sandstone in the UK southern North Sea. International Journal of Greenhouse Gas Control, 9:220–233.

O'Sullivan, M. J., Pruess, K., and Lippmann, M. J. (2001). State of the art of geothermal reservoir simulation. Geothermics, 30(4):395 – 429.

Petra, C. G., Schenk, O., & Anitescu, M. (2014a). Real-time stochastic optimization of complex energy systems on high-performance computers. Computing in Science & Engineering, 16(5), 32-42.

Petra, C. G., Schenk, O., Lubin, M., & Gärtner, K. (2014b). An augmented incomplete factorization approach for computing the Schur complement in stochastic optimization. SIAM Journal on Scientific Computing, 36(2), C139-C162.

Pruess, K., Oldenburg, C., and Moridis, G. (1999). Tough2 user's guide version 2. Lawrence Berkeley National Laboratory.

Rin, R., Tomin, P., Garipov, T., Voskov, D. & Tchelepi, H. A. (2017). General Implicit Coupling Framework for Multi-Physics Problems. In SPE reservoir simulation symposium. Society of Petroleum Engineers.

Rutqvist, J., Wu, Y. S., Tsang, C. F., & Bodvarsson, G. (2002). A modeling approach for the analysis of coupled multiphase fluid flow, heat transfer, and deformation in fractured porous rock. International Journal of Rock Mechanics and Mining Sciences, 39(4), 429-442.

Schenk, O., & Gärtner, K. (2004). Solving unsymmetric sparse systems of linear equations with PARDISO. Future Generation Computer Systems, 20(3), 475-487.

Schenk, O., & Gärtner, K. (2006). On fast factorization pivoting methods for sparse symmetric indefinite systems. Electronic Transactions on Numerical Analysis, 23(1), 158-179.

Settari, A., & Mourits, F. M. (1998). A coupled reservoir and geomechanical simulation system. SPE Journal, 3(03), 219-226.

Jenny, P., Tchelepi, H. A., & Lee, S. H. (2009). Unconditionally convergent nonlinear solver for hyperbolic conservation laws with S-shaped flux functions. Journal of Computational Physics, 228(20), 7497-7512.

Trangenstein, J. A. (1989). Analysis of a model and sequential numerical method for thermal reservoir simulation. In ECMOR I-1st European Conference on the Mathematics of Oil Recovery.

Stanford Geothermal Program, (1980). Proceedings of the special panel on geothermal model study, report SGP-TR-42. Energy Resources Engineering, Stanford University.

Wang, X., & Tchelepi, H. A. (2013). Trust-region based solver for nonlinear transport in heterogeneous porous media. Journal of Computational Physics, 253, 114-137.

Wong, Z. Y., Horne, R., & Voskov, D. (2015). A Geothermal Reservoir Simulator in AD-GPRS. In Proceedings World Geothermal Congress 2015.

Wong, Z. Y., Horne, R., & Voskov, D. (2016) Comparison of Nonlinear Formulations for Geothermal Reservoir Simulations. 41st Workshop on Geothermal Reservoir Engineering.

Van Odyck, D. E., Bell, J. B., Monmont, F., & Nikiforakis, N. (2009). The mathematical structure of multiphase thermal models of flow in porous media. In Proceedings of the Royal Society of London A: Mathematical, Physical and Engineering Sciences (Vol. 465, No. 2102, pp. 523-549). The Royal Society.

Voskov, D. V., and Tchelepi, H. A. (2012). Comparison of nonlinear formulations for two-phase multi-component EOS based simulation. Journal of Petroleum Science and Engineering, 82:101–111.

Voskov, D., Zhou, Y., and Volkov, O. (2012). Technical description of AD-GPRS. Energy Resources Engineering, Stanford University.

Voskov, D., Zaydullin, R., and Lucia, A. (2016). Heavy oil recovery efficiency using SAGD, SAGD with propane co-injection and STRIP-SAGD. Computers & Chemical Engineering, 88:115–125.

Zaydullin, R., Voskov, D. V., James, S. C., Henley, H., & Lucia, A. (2014). Fully compositional and thermal reservoir simulation. Computers & Chemical Engineering, 63, 51-65.

Zhou, Y. (2012). Parallel general-purpose reservoir simulation with coupled reservoir models and multisegment wells. Ph.D. thesis, Stanford University.

Zhou, Y., Jiang, Y., and Tchelepi, H. A. (2013). A scalable multistage linear solver for reservoir models with multisegment wells. Computational Geosciences, 17(2):197–216.

APPENDIX A

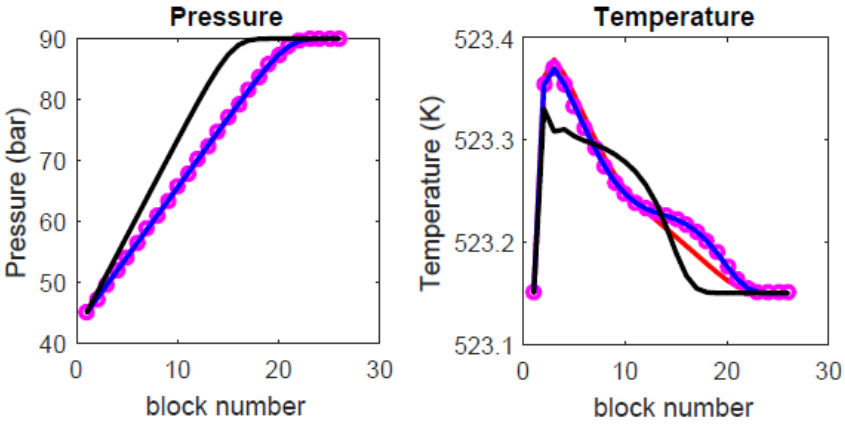

Figure 4: Pressure (bar) and temperature (K) for the blocks in the single-phase production scenario (black line: constant density, blue line: constant pressure, magenta dots: hybrid, red line: fully coupled)

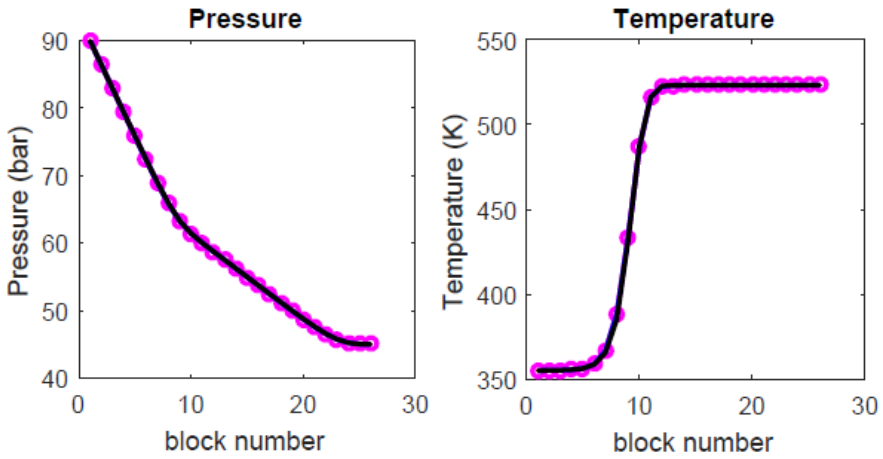

Figure 5: Pressure (bar) and temperature (K) for the blocks in the single-phase injection scenario (black line: constant density, blue line: constant pressure, magenta dots: hybrid, red line: fully coupled)

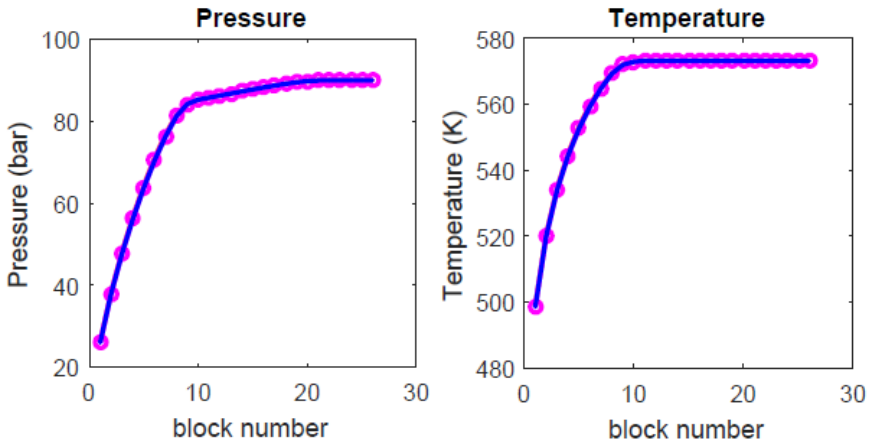

Figure 6: Pressure (bar) and temperature (K) for the blocks in the two-phase production scenario (black line: constant density, blue line: constant pressure, magenta dots: hybrid, red line: fully coupled)

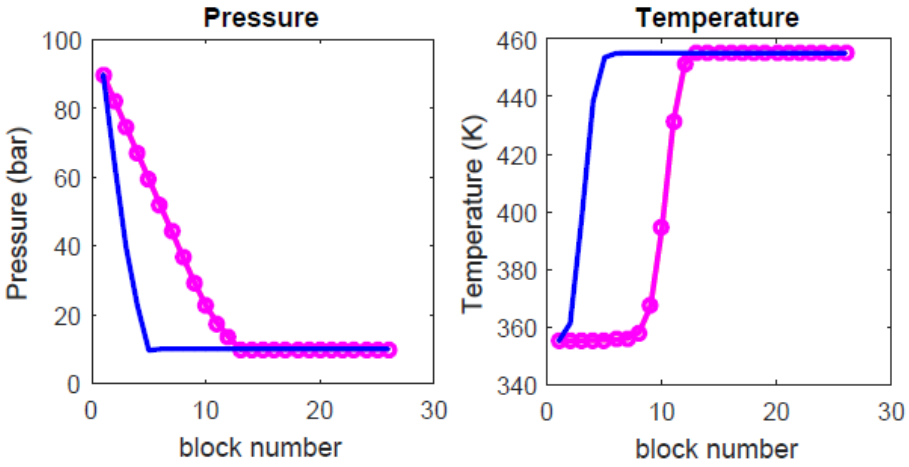

Figure 7: Pressure (bar) and temperature (K) for the blocks in the two-phase production scenario (black line: constant density, blue line: constant pressure, magenta dots: hybrid, red line: fully coupled)

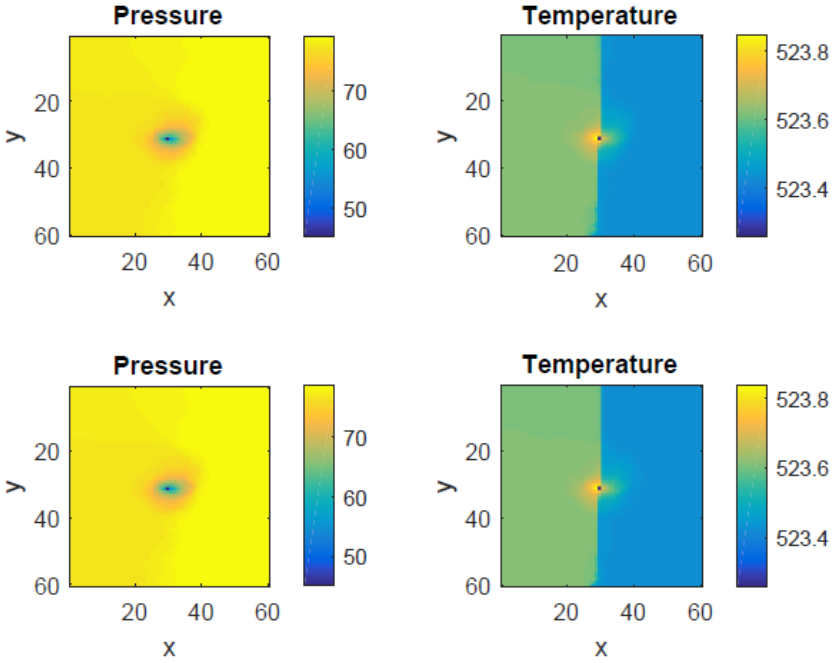

Figure 8: Pressure (bar) and temperature (K) profile for two-dimensional production case fully implicit (top) and hybrid (bottom)

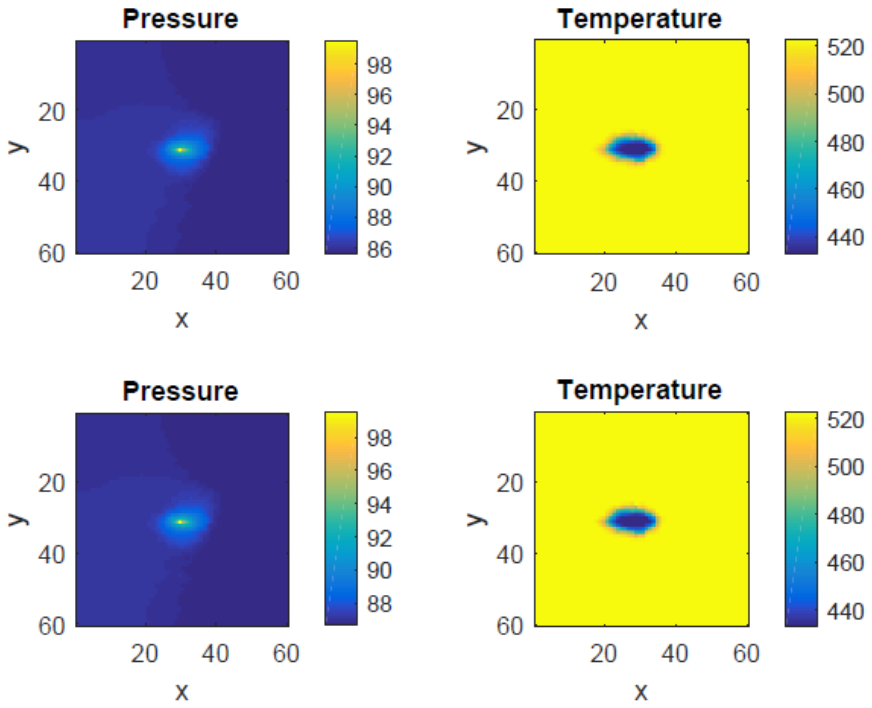

Figure 9: Pressure (bar) and temperature (K) profile for two-dimensional injection case fully implicit (top) and hybrid (bottom)